Dynamic Responses of an Atomic Force Microscope Interacting With Samples

Jih-Lian Ha

Associate Professor
Department of Mechanical Engineering,
Far East College,
49 Chung-Hua Road,
Shin-Shi, Tainan, Taiwan 744, ROC

Rong-Fong Fung[1]

Professor
e-mail: rffung@ccms.nkfust.edu.tw

Yi-Chan Chen

Graduate Student

Department of Mechanical and Automation Engineering,
National Kaohsiung First University of Science
and Technology,
1 University Road, Yenchau,
Kaohsiung, Taiwan 824, ROC

The objective of this paper is to formulate the equations of motion and to analyze the vibrations of an atomic force microscope (AFM), which contains a piezoelectric rod coupling with a cantilever beam, and the tip mass interacting with samples. The governing equations of the AFM system are formulated completely by Hamilton's principle. The piezoelectric rod is treated as an actuator to excite the cantilever beam via an external voltage. The repulsive forces between the tip and samples are modeled by the Hertzian, the Derjaguin-Müller-Toporov, and Johnson-Kendall-Roberts models in the contact region. Finally, numerical results are provided to illustrate the coupling effects between the piezoelectric actuator and the cantilever beam and the interaction effects between the tip and samples on the dynamic responses.
[DOI: 10.1115/1.2101851]

1 Introduction

The atomic force [1] between the tip and sample of the atomic force microscope (AFM) is employed during the process of measurement. Some important observations of the AFM were made from the governing equations and boundary conditions [2], wherein a complete actuating force called the interatomic *Lennard-Jones* force was obtained from the *Lennard-Jones* or "6-12" potential. The cantilevers have made it possible to build new sensors, which are simple, compact, and easy to operate for measuring materials.

The AFM force-distance curves have become a fundamental tool in several fields of research, such as surface science, material engineering, and biochemistry. Furthermore, they have great importance for the studies of surface interactions from a theoretical point of view [3]. The contact and noncontact models of the AFM [2] corresponding to the tip-sample interaction in the form of the repulsive and attraction forces, respectively, were employed to measure the sample's topography. In these cases, the tip is close to, but not really in contact with, the sample surface.

In the applications of the AFM to measure all materials, from large rigid sphere with high surface energies to small compliant bodies with low surface energies, many contact-force models must be employed. The contact stiffness was measured by using the atomic force acoustic microscopy [4], wherein the Hertzian (HZ) contact model based on the sensor tip as a sphere was used to approximate the tip-sample force law. The Johnson-Kendall-Roberts (JKR) contact theorem [5] was used for probing trace amounts of surface contamination. In the Derjaguin-Müller-Toporon (DMT) model [6], the elastic sphere is deformed according to the HZ model. In these previous researches [4–6], the dynamics of the AFM is not considered.

The previous researches [2–6] do not consider either the coupling effects between the piezoelectric actuator (PEA) and the cantilever beam or the interaction forces between the tip and samples. In this paper, the dynamic modeling of the PEA and cantilever beam is different from the previous papers, which analyzed the AFM statically [7], modeled the composite cantilever beam without a PEA at the base [2], and modeled the cantilever beam and its tip mass as an equivalent spring and lumped mass system [8]. Most of the papers [2,7,8] concerning the dynamic responses of the AFM assumed only a base excitation without considering the dynamic coupling between the PEA and cantilever beam.

2 Dynamic Formulation

Figure 1(*a*) shows the schematic draw of the AFM system, which consists of a PEA coupling with a cantilever beam associated with a pyramid rigid tip mass. The geometric dimensions are shown in Fig. 1(*b*), where the subscripts *p* and *b* are used for the PEA and the cantilever beam, respectively. The detailed material properties and geometric dimensions are listed in Table 1. The tip mass has height h, thickness 2ℓ, and width w. The distance between the point Q and the geometric center H of the tip mass is e. It is noted that the dynamic modeling of the PEA and cantilever beam is coupled in this paper.

2.1 Kinetic and Strain Energies. In the dynamic modeling analysis, a fixed coordinate system (OXZ), describing the PEA, and a moving coordinate system (oxz) attached on the top of the PEA, describing the cantilever beam, are adopted to describe the AFM system as shown in Fig. 1(*b*). The deformed position vector of an arbitrary point P of the PEA is

$$\mathbf{R}_p(Z,t) = [Z + u(Z,t)]\mathbf{k}, \qquad (1)$$

where $u(Z,t)$ represents the axial deformation of the PEA along the Z axis. The deformed position vector of an arbitrary point A with the position coordinate $(x, \ell_p + z)$ of the cantilever beam measured from the fixed coordinate system is

$$\mathbf{R}_A(x,z,t) = [x - zv_x(x,t)]\mathbf{i} + [\ell_p + z + u(\ell_p,t) + v(x,t)]\mathbf{k}, \quad (2)$$

where $v(x,t)$ represents the transverse deflection of the cantilever beam, $u(\ell_p,t)$ describes the deformation of the PEA at the top point $Z = \ell_p$, and $\mathbf{i}$ and $\mathbf{k}$ are the unit vectors of the fixed coordinate system (OXZ). The deformed position vector of the mass center H with the position coordinate $(\ell_b + \ell, \ell_p - e)$ of the pyramid rigid tip mass is

$$\mathbf{R}_H(\ell_b + \ell, \ell_p - e, t) = (\ell_b + \ell)\mathbf{i} + [\ell_p - e + u(\ell_p,t) + v(\ell_b,t)$$
$$+ \ell v_x(\ell_b,t)]\mathbf{k}. \qquad (3)$$
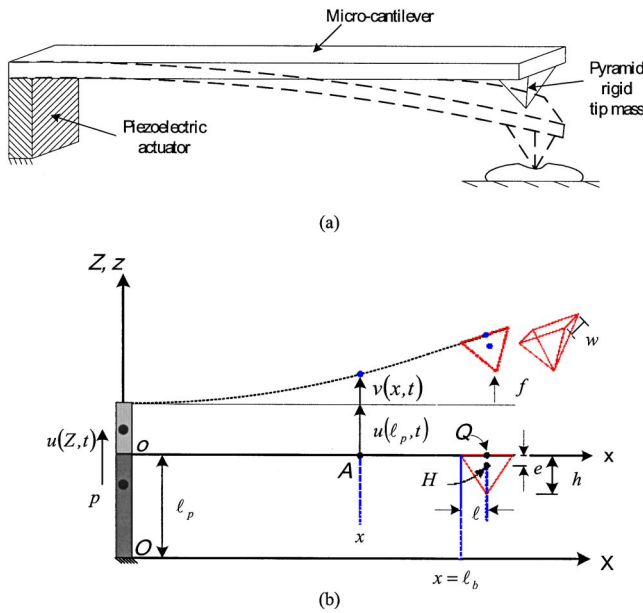
Therefore, the total kinetic energy of the AFM system is

Fig. 1 Schematic diagrams of (a) the cantilever beam with a PEA and (b) the deformed configuration of the AFM system

$$T = \frac{1}{2}\int_{V_p} \rho_p \frac{d}{dt}\mathbf{R}_p \cdot \frac{d}{dt}\mathbf{R}_p dV_p + \frac{1}{2}\int_{V_b} \rho_b \frac{d}{dt}\mathbf{R}_A \cdot \frac{d}{dt}\mathbf{R}_A dV_b$$

$$+ \frac{1}{2}m\frac{d}{dt}\mathbf{R}_H \cdot \frac{d}{dt}\mathbf{R}_H$$

$$= \frac{1}{2}\int_0^{\ell_p} \rho_p A_p u_t^2(Z,t)dZ + \frac{1}{2}\int_0^{\ell_b} \rho_b A_b [u_t(\ell_p,t) + v_t(x,t)]^2 dx$$

$$+ \frac{1}{2}m[u_t(\ell_p,t) + v_t(\ell_b,t) + \ell v_{xt}(\ell_b,t)]^2, \qquad (4)$$

where ρ_p and ρ_b are the mass densities of the PEA and cantilever

beam, respectively, A_p and A_b are their uniform cross-sectional areas, and m is the tip mass.

The Lagrangian strains of the cantilever beam and PEA are respectively as follows:

$$\text{Cantilever beam:} \varepsilon_{b11} = -zv_{xx}, \quad \varepsilon_{b13} = \varepsilon_{b31} = v_x, \qquad (5a)$$

$$\text{Piezoelectric actuator:} \varepsilon_{p33} = u_Z, \quad \varepsilon_{p13} = \varepsilon_{p31} = 0, \qquad (5b)$$

where the cantilever beam is described by Euler beam theory.

One-dimensional constitutive equation of the PEA can be written as

$$\begin{bmatrix} \sigma_{p33} \\ E \end{bmatrix} = \begin{bmatrix} E_p & -h_{33} \\ -h_{33} & \beta_{33} \end{bmatrix} \begin{bmatrix} \varepsilon_{p33} \\ D_{33} \end{bmatrix}, \qquad (5c)$$

where D_{33} and E_p are the electrical displacement and Young's modulus of the PEA, respectively; ε_{p33} and σ_{p33} are the mechanical strain and stress along the Z direction, respectively. E is the electric field induced by the PEA, β_{33} is the dielectric constant, and h_{33} is the piezoelectric constant.

The total potential energy of the AFM system is

$$U = \frac{1}{2}\int_{V_p} (\sigma_{p33}\varepsilon_{p33} + D_{33}E)dV_p + \frac{1}{2}\int_{V_b} \sigma_{b11}\varepsilon_{b11} dV_b$$

$$= \frac{1}{2}\int_0^{\ell_p} [E_p A_p u_Z^2(Z,t) - 2h_{33}A_p D_{33}(Z,t)u_Z(Z,t)$$

$$+ A_p\beta_{33}D_{33}^2(Z,t)]dZ + \frac{1}{2}\int_0^{\ell_b} [E_b I_b v_{xx}^2(x,t)]dx, \qquad (6)$$

where $I_b = \int z^2 dA_b$ and E_b is Young's modulus of the cantilever beam.

Due to the input voltage $V_{in}(t) = \int_0^{\ell_p} E\,dZ$ is applied along the Z direction of the PEA, the virtual work due to the input voltage and the interaction force f between the tip and sample can be expressed as

$$\delta W = f\delta[v(\ell_b,t) + \ell v_x(\ell_b,t)] + \int_0^{\ell_p} A_p E \delta D_{33}(Z,t)dZ. \qquad (7)$$

Table 1 Material properties and geometric dimensions of the AFM system

	Piezoelectric actuator	Silicon beam	Tip mass
Young's Modulus (N/m^2):	$E_p = 2.216\times10^{10}$	$E_b = 7.03\times10^{10}$	
Density (kg/m^3):	$\rho_p = 8000$	$\rho_b = 2500$	
h_{33} ($N/Coulomb$):	5.45136×10^8		
β_{33} ($V-m/Coulomb$):	7.81×10^7		
Length (μm):	$\ell_p = 4000$	$\ell_b = 174$	$2\ell = 10$
Width (μm):	$w_p = 500$	$w_b = 39$	$w = 10$
Thickness (μm):	$t_p = 500$	$t_b = 6.9$	
Height (μm):			$h = 10$

2.2 Hamilton's Principle. By substituting Eqs. (4), (6), and (7) into Hamilton's principle

$$\int_{t_1}^{t_2} [\delta(T-U) + \delta W] dt = 0, \tag{8}$$

one obtains the governing equations for the AFM system [2] as follows:

$$\rho_p A_p u_{tt}(Z,t) - E_p A_p u_{ZZ}(Z,t) = 0, \quad 0 < Z < l_p \tag{9}$$

$$\rho_b A_b v_{tt}(x,t) + E_b I_b v_{xxxx}(x,t) = -\rho_b A_b u_{tt}(\ell_p,t), \quad 0 < x < l_b, \tag{10}$$

$$-h_{33} A_p u_Z(Z,t) + A_p \beta_{33} D_{33}(Z,t) = A_p E, \quad 0 < Z < l_p, \tag{11}$$

and the associated boundary conditions are

$$u(0,t) = 0, \tag{12a}$$

$$E_p A_p u_Z(l_p,t) - h_{33} A_p D_{33}(l_p,t) + E_b I_b v_{xxxx}(0,t) + m\lfloor u_{tt}(l_p,t)$$
$$+ lv_{xtt}(l_b,t) + v_{tt}(l_b,t)\rfloor + \rho_b A_b l_b u_{tt}(l_p,t) = 0, \tag{12b}$$

$$v_x(0,t) = 0, \tag{12c}$$

$$m[v_{tt}(l_b,t) + lv_{xtt}(l_b,t)] - E_b I_b v_{xxx}(l_b,t) = -mu_{tt}(l_p,t) + f, \tag{12d}$$

$$m[l^2 v_{xtt}(l_b,t) + lv_{tt}(l_b,t)] + E_b I_b v_{xx}(l_b,t) = -mlu_{tt}(l_p,t) + fl. \tag{12e}$$

In the geometric model, it is a fact that the top point $Z = \ell_p$ of the PEA has the same deflection as that of the base point $x = 0$ of the cantilever beam. Thus, in the manipulation of Hamilton's principle, we have used the following continuous condition:

$$u(\ell_p,t) = v(0,t), \tag{13}$$

which enables the coefficients of $\delta u(l_p,t)$ and $\delta v(0,t)$ to be added together, and Eq. (12b) is obtained.

3 The Interaction Forces Between the Tip and Samples

In the limit of high loads or low surface forces, an AFM experiment can follow the HZ model. The JKR model is suitable for the highly adhesive systems with low stiffness and large tip radii [5]. The DMT model is applicable for systems with low adhesion forces and small tip radii.

3.1 The Hertzian Contact-Force Model. In the Hertzian model [9], the tip is considered as a smooth elastic sphere, while the sample is a rigid flat surface. The Hertzian contact-force model takes into account neither surface forces nor adhesion forces. Thus, we have the adhesion or pull-off force $f_{ad} = 0$. Some associated equations can be expressed as follows:

$$a_{HZ} = \sqrt[3]{\frac{Rf}{K}}, \tag{14a}$$

$$\delta = \frac{a_{HZ}^2}{R}, \tag{14b}$$

where a_{HZ} is the contact radius in Fig. 2, R is the radius of a sphere, f is the loading force pressed onto a flat surface, δ is the deformation of the spherical tip, and K is the reduced Young's modulus as follows:

$$\frac{1}{K} = \frac{3}{4}\left[\left(\frac{1-\nu_{tip}^2}{E_{tip}}\right) + \left(\frac{1-\nu_{sample}^2}{E_{sample}}\right)\right], \tag{15}$$

where E_{tip} and E_{sample} are the Young's modulus, and ν_{tip} and
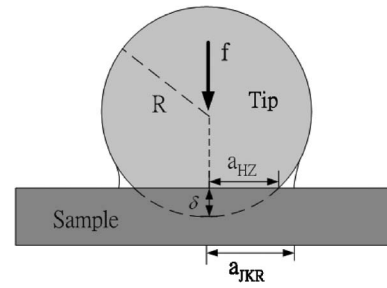

Fig. 2 Deformation of a sphere on a flat surface following the HZ and JKR models, where f is the loading force, R is the radius of the sphere, δ is the deformation of the spherical tip, and a_{HZ} and a_{JKR} are the contact radii. of the HZ and JKR models, respectively. The profile of the spherical tip in the DMT model is the same as that in the HZ model.

ν_{sample} are the Poisson ratios of the tip and sample, respectively.

The contact radius a_{HZ} can be calculated from Eq. (14b) if δ and R are known, while the reduced Young's modulus K can be obtained from Eq. (15) if the E_{tip}, E_{sample}, ν_{tip}, and ν_{sample} are known. Substituting a_{HZ} and K into Eq. (14a), we obtain the interaction force f between the tip and sample for the Hertzian contact-force model.

3.2 The JKR Contact-Force Model. The JKR model [8] neglects the long-range forces outside the contact region, but only considers the short-range forces inside the contact region. With the JKR assumptions, the contact radius a_{JKR}, the adhesion force f_{ad}, and the deformation δ of the spherical tip can be modified as follows:

$$a_{JKR} = \sqrt[3]{\frac{R}{K}[f + 3\pi Rw + \sqrt{6\pi Rwf + (3\pi Rw)^2}]}, \tag{16a}$$

$$\delta = \frac{a_{JKR}^2}{R} - \frac{2}{3}\sqrt{\frac{6\pi w a_{JKR}}{K}}, \tag{16b}$$

$$f_{ad} = \frac{3}{2}\pi Rw, \tag{16c}$$

where w is the surface energy, which is given for the sample.

3.3 The DMT Contact-and Non-Contact-Force Models. Without the external loading, the DMT model [10] takes into account the interaction forces between the tip and sample outside the contact region. These forces produce a finite area of contact. The contact radius a, the adhesion force f_{ad}, the deformation δ of the
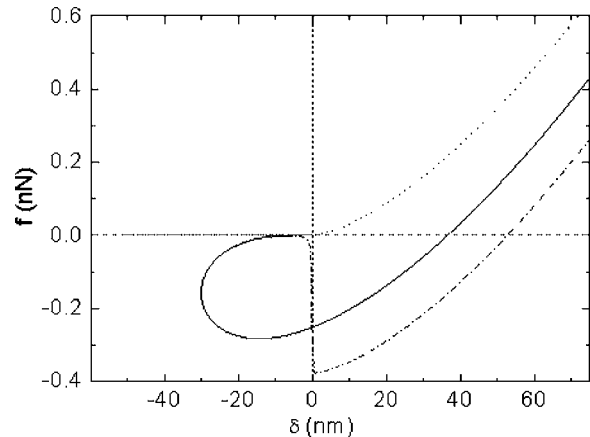

Fig. 3 The relationships between the interaction forces and the deformations of the spherical tip. ($\cdots$ HZ; --- DMT; — JKR)
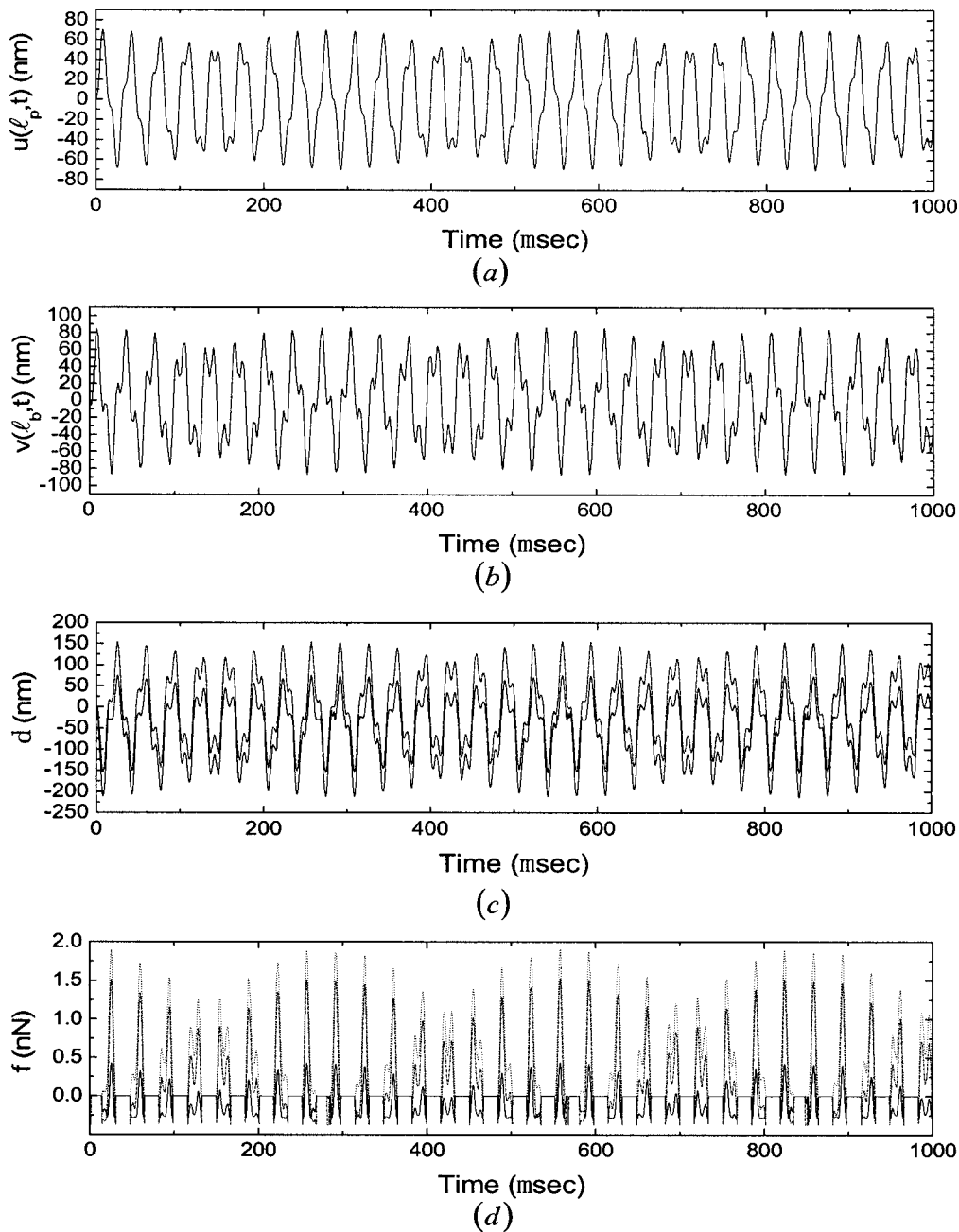
Fig. 4 The diagram of the cantilever beam system with three atomic force models. (*a*) The displacement of the PEA at the end. (*b*) The displacement of the cantilever beam at the end. (*c*) The distance between the tip and the sample. (*d*) The relations of the atomic force and time. ($\cdots$ HZ; --- DMT; — JKR)

spherical tip, and the distance D between the spherical tip and the samples are found by minimizing the sum of the elastic and surface energies as follows:

$$a = \sqrt[3]{\frac{R}{K}(f + 2\pi Rw)}, \qquad (17a)$$

$$\delta = \frac{a^2}{R} - \frac{2}{3}\sqrt{\frac{6\pi wa}{K}}, \qquad (17b)$$

$$f_{ad} = 2\pi Rw, \qquad (17c)$$

$$f = -2\pi Rw/(1 - D/D_0)^2, \qquad (18)$$

where D_0 is the initial distance of D.

In the DMT approximation, the adhesion forces are taken into account, but the elastic sphere is deformed according to the HZ model, and the adhesion forces would not deform the sample surfaces [10]. Thus, we have $a = a_{HZ}$ in Fig. 2, and the profile of the spherical tip in the DMT model is the same as that in the HZ model.

3.4 The Interaction Force and Deformation. The relationships between the interaction forces and the deformations of the spherical tip for the above three force models are compared in Fig. 3. It can be observed that the values of the interaction forces and the deformations of the spherical tip are always positive in the HZ

model. The attractive forces (negative values) are considered in the JKR and DMT models rather than in the HZ model. In the JKR model, the short-range force is considered and the interaction force is a two-valued function corresponding to a deformation δ of the spherical tip, which is referred to as the hysteretic behavior. The adhesion hysteresis [11] has been discussed for the relationship between the adhesion and friction forces. In the DMT model, the adhesion forces are taken into account, but the profile of the spherical tip is assumed to be Hertzian, as if adhesion forces could not deform the sample's surfaces.

4 Numerical Results

In order to transform partial differential equations into ordinary differential equations, the coupled system is divided into two regions: the PEA $0 < Z < \ell_p$ and the cantilever beam $0 < x < \ell_b$. By using the standard finite element method [2] and assembling equations of motion, we obtain a set of ordinary differential equations. The material properties and geometric dimensions [4] of the PEA and the cantilever beam with a tip mass are listed in Table 1. Numerical simulations of the AFM system are presented for the three contact-force models with integration error 10^{-12} m of Runge-Kutta method. The zero initial conditions, $\mathbf{Q}(0)=\mathbf{0}$ and $\dot{\mathbf{Q}}(0)\mathbf{0}$, are adopted for the forced vibrations, which are caused by the harmonic excitations of the PEA.

In the numerical simulations of the AFM system with the interaction forces, the applied voltage $V_{in}(t)=15 \sin \omega t$ V with $\omega =30$ kHZ is employed. In the HZ model, the Young's modulus of the sample E_{sample} is 100 kPa [12], and the Poisson ratios of the tip and sample are taken as 0.28 and 0.5, respectively. By using Eq. (15), the reduced Young's modulus K is obtained as 1.8 $\times 10^5$ N/m^2. The surface energy w is taken as 2 mJ/m^2 in the JKR and DMT models [10]. The tip radius R of the silicon cantilever beam is 30 nm, and the initial distance between the tip and sample is 0.3 nm.

The displacements $u(l_p,t)$ at the top point of the PEA and the $v(l_b,t)$ at the tip point of the cantilever beam under the interaction forces of the three contact-force models are almost the same as shown in Figs. 4(a) and 4(b), respectively. However, the deformation δ of the spherical tip is about 75 nm via the JKR model and is only one-half of those via the DMT and HZ models as shown in Fig. 4(c). The interaction forces of the three contact-force models are shown in Fig. 4(d), where the repulsive force (positive value) is the maximum about 1.8 nN for the HZ model, is about 1.5 nN for the DMT model, and is the minimum about 0.4 nN for the JKR model.

5 Conclusions

Both the coupling effects between the PEA and the cantilever beam and the interaction forces between the tip and samples are involved in the dynamic formulations, which are the main merits of this paper. Due to various levels of loads, surface energies, adhesive forces, stiffnesses, and tip radii, three contact-force models are considered for the AFM measurements in this paper. From the dynamic formulation and numerical results, the following conclusions can be drawn:

1. The accelerations of the base excitations of the noncoupled system are almost the same as those at the top point of the PEA of the coupled system. However, the responses of the cantilever tip of the coupled system are much larger than those of the noncoupled system. This enables the coupled AFM system to have the high quality factor and high sensitivity in measurements of samples.
2. The displacements at the top point of the PEA and those at the tip point of the cantilever beam under the interaction forces of the three contact-force models are almost the same. However, the deformations of the spherical tip are quite different for the three contact-force models.

References

[1] Binning, G., Quate, C. F., and Gerber, C., 1986, "Atomic Force Microscope," Phys. Rev. Lett., **56**, pp. 930–933.
[2] Fung, R. F., and Huang, S. C., 2001, "Dynamic Modeling and Vibration Analysis of the Atomic Force Microscope," ASME J. Vibr. Acoust., **123**, pp. 502–509.
[3] Cappella, B., and Dietler, G., 1999, "Force-Distance Curves by Atomic Force Microscopy," Surf. Sci. Rep., **34**, pp. 1–104.
[4] Amelio, S., Goldade, A. V., Rabe, U., Bhushan, B., and Arnold, W., 2001, "Measurements of elastic properties of ultra-thin diamond-like carbon using atomic force acoustic microscopy," Thin Solid Films, **392**, pp. 75–84.
[5] Johnson, K. J., Kendall, K., and Roberts, A. D., 1971, "Contact Mechanics," Proc. R. Soc. London, Ser. A, **324**, p. 301.
[6] Derjaguin, B. V., Muller, V. M., and Toporov, Yu. P., 1975, "Effect of Contact Deformations on the Adhesion of Particles," J. Colloid Interface Sci., **53**(2), pp. 314–326.
[7] Itoh, T., and Suga, T., 1994, "Piezoelectric Sensor for Detecting Force Gradients in Atomic Force Microscopy," Jpn. J. Appl. Phys., Part 1, **33**, pp. 334–340.
[8] Ashhab, M., Salapaka, M. V., Dahleh, M., and Mezic, I., 1999, "Dynamical Analysis and Control of Microcantilever," Automatica, **35**, pp. 1663–1670.
[9] Hertz, H., 1882, "Uber Die Beruhrung Feater Elastischer Korper," J. Reine Angew. Math., **92**, pp. 156–171.
[10] Maugis, D., 1992, "Adhesion of Spheres: The JKR-DMT Transition Using a Dugdale Model," J. Colloid Interface Sci., **150**(1), pp. 243–269.
[11] Frantz, P., Artsyukhovich, A., Carpick, R. W., and Salmeron, M., 1997, "Use of capacitance to measure surface forces. 2. Application to the study of contact mechanics," Langmuir, **13**, pp. 5957–5961.
[12] Radmacher, M., 1997, "Measuring the Elastic Properties of Biological Sample with the AFM," IEEE Eng. Med. Biol. Mag., **16**, pp. 47–57.